JOURNAL OF GEOPHYSICAL RESEARCH, VOL. 88, NO. B6, PAGES 4997-5008, JUNE 10, 1983

Eruption Age of a Pleistocene Basalt From ^{40}Ar-^{39}Ar Analysis of Partially Degassed Xenoliths

A. R. GILLESPIE,[1] J. C. HUNEKE,[2] AND G. J. WASSERBURG

The Lunatic Asylum of the Charles Arms Laboratory, Division of Geological and Planetary Sciences, California Institute of Technology, Pasadena, California 91125

We have applied ^{40}Ar-^{39}Ar dating to potassium-rich granitic xenoliths and host basalt from the Pleistocene Big Pine volcanic field, California. These xenoliths had been partially degassed upon their inclusion in the basaltic lava. Argon released from the xenoliths at extraction temperatures below ~900°C yielded plateau ages indistinguishable from the total K-Ar age of the basalt. The best estimate of the age of eruption was 1.18 ± 0.05 (2σ) m.y. ^{40}Ar extracted at higher temperatures included radiogenic argon not degassed from the late Cretaceous xenoliths 1.18 m.y. ago, causing an increase in the apparent age for the high-temperature fractions. The agreement of the low-temperature xenolith plateau ages and the basalt K-Ar ages demonstrates that ^{40}Ar-^{39}Ar analysis of xenoliths may be used to measure the age of eruption of very young lavas. This is significant because in many instances ages cannot be reliably determined by analysis of the lavas themselves.

1. INTRODUCTION

We have applied the stepwise degassing variant of the ^{40}Ar-^{39}Ar dating method to granitic xenoliths of Cretaceous age from a Pleistocene basalt. This was done to establish whether there exist plateaus in the ^{40}Ar-^{39}Ar age spectra that correspond to the time of heating of the xenolith in the host magma, with the intent to develop and demonstrate a new technique for accurately dating the eruption of very young lavas. The theoretical basis for this approach was explored in a previous study [*Gillespie et al.*, 1982]. It was shown that if xenoliths were of Cretaceous age or younger, then age plateaus extending over 25% or more of the total ^{39}Ar released and giving the age of eruption could be realistically anticipated. The development of an eruption-age plateau requires a reasonably wide disparity in the diffusion parameters and/or activation energy for Ar diffusion from K-bearing sites in the xenolith, coupled with sufficient degassing of the xenolith in the magma.

Accurate dating of K-poor basic lavas is necessary for the study of many Quaternary geological processes. This research was part of a study of Pleistocene glacial chronology in the southeastern Sierra Nevada near Independence, Inyo County, California [*Gillespie*, 1982]. Here, as remarked by *Knopf* [1918] and *Moore* [1963], basalts of the Big Pine volcanic field interfinger with late Pleistocene moraines. Dating of the intercalated basalts should provide limits to the ages of the glacial advances. *Dalrymple* [1964*a*] and *Dalrymple et al.* [1982] have dated one of these basalts by conventional K/Ar analysis and obtained ages of 0.06 ± 0.10 and 0.09 ± 0.18 m.y. and 0.05 ± 0.09 m.y., respectively (uncertainties are 2σ). These results only place bounds on the ages and do not establish the firm age relationships that are necessary for studying such young geological events. It was to improve the accuracy of dates for such young lavas that we have explored the possibility of ^{40}Ar-^{39}Ar dating of the granitic xenoliths included in the basalts. In this paper we discuss the results of ^{40}Ar-^{39}Ar analyses of xenoliths and host basalts from the oldest flow in the same volcanic field, for which accurate K/Ar ages could be more easily obtained. In a subsequent paper we will present the analyses of xenoliths from the extremely young lava studied by *Dalrymple* [1964*a*] and *Dalrymple et al.* [1982].

1.1 *Conventional K/Ar Dating*

There are formidable obstacles to the precise and accurate dating of young basic lavas by conventional K/Ar methods. One of these is the presence of Ar dissolved in the magma. Such Ar trapped in the basalt may mask the very small amounts of radiogenic ^{40}Ar (hereinafter denoted by superscript asterisk) found in young rocks. Furthermore, the isotopic composition ($^{36}Ar/^{40}Ar$) of the trapped Ar (hereinafter denoted by subscript t) is a priori unknown and is not determined by conventional K/Ar analysis. Especially for young, K-poor rocks with small amounts of $^{40}Ar^*$, the apparent K/Ar age is quite sensitive to the assumed $(^{36}Ar/^{40}Ar)_t$.

A second obstacle to K/Ar dating is the presence in many lavas of microscopic fragments of ancient country rock rich in K. Basalts of the Big Pine volcanic field, for example, are extensively contaminated by granitic xenoliths from the Mesozoic plutons through which the lavas erupted (Figure 1). Such fragments may contain large amounts of $^{40}Ar^*$ incompletely degassed from the fragment when incorporated in the lava (hereinafter denoted by $^{40}Ar_0^*$). If incompletely degassed xenocrysts occur in the lava analyzed, the apparent eruption age of the lava will be too great.

Although the temperature of xenocrysts incorporated into basaltic magma at the time of eruption rises to ~1100°C within seconds and can remain this high for more than a day while the lava flow solidifies, evidently not all the $^{40}Ar_0^*$ is diffused from the xenocryst. *Dalrymple* [1964*b*] has demonstrated Ar retention of ~2.5% in a 10-cm-diameter granitic clast found 3 m below the top of a 25-m-thick basalt flow. Because the characteristic dimension of diffusion seems to be determined not by xenolith diameter but rather by individual grain size or the width of exsolution lamellae, even individual microscopic xenocrysts dispersed throughout the magma will probably be similarly retentive. It is generally not possible to eliminate nor even to detect the presence of individual xenocrysts during preparation of samples for K/Ar analysis.

1.2 *^{40}Ar-^{39}Ar Dating*

The stepwise heating ^{40}Ar-^{39}Ar method [*Merrihue and Turner*, 1966; *Turner*, 1970, 1971] ameliorates many problems

[1] Now at Jet Propulsion Laboratory, Pasadena, California 91109.
[2] Now at Charles Evans and Associates, San Mateo, California 94402.

Paper number 3B0439.
0148-0227/83/003B-0439$05.00

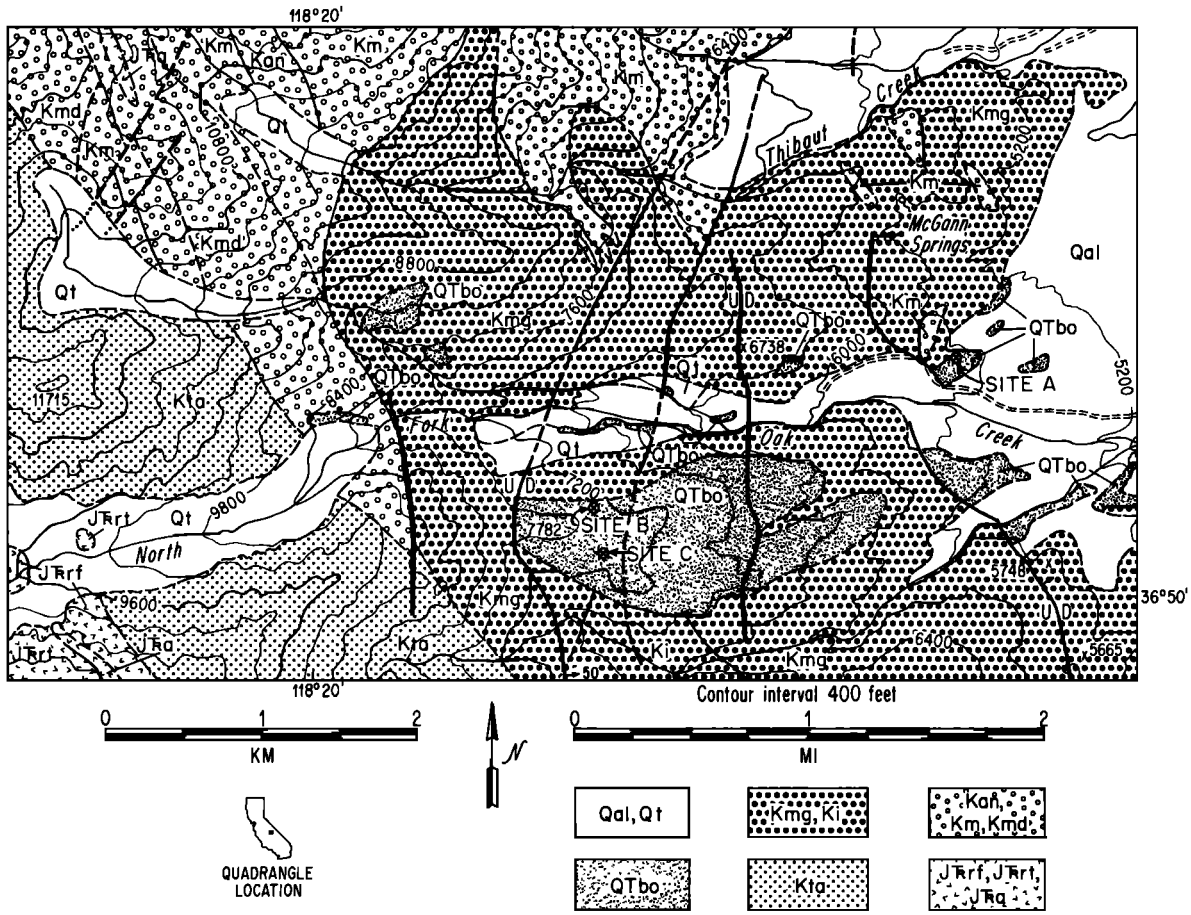

Fig. 1. Sample locations and generalized geology, after *Moore* [1963]. Qal and Qt are Quaternary fan and stream gravels and Quaternary glacial deposits, respectively. Pleistocene basalts are designated QTbo. Two Cretaceous quartz monzonites (heavy stipple) are shown; the McGann pluton (Kmg) is widespread, while the Independence pluton (Ki) crops out only in the south. The Cretaceous Tinnemaha granodiorite (KTa) is found only west of the faults along which the basalt is thought to have extruded. Kan, Km, and Kmd (open circles) are anorthosites, diorites, and gabbros of early Cretaceous age. Jurassic-Triassic volcanic rocks (JTRrf, JTRrt, JTRq) were metamorphosed at the time of the Cretaceous intrusions. Topographic data are from the Mount Pinchot Quadrangle, Inyo County, California (1953).

encountered in K/Ar dating. If $^{40}Ar^*$ and Ar_r are contained in phases or sites with different retentivities, the resultant separation of the two types of Ar during stepwise thermal extraction may in principle permit the determination of $(^{36}Ar/^{40}Ar)_r$,

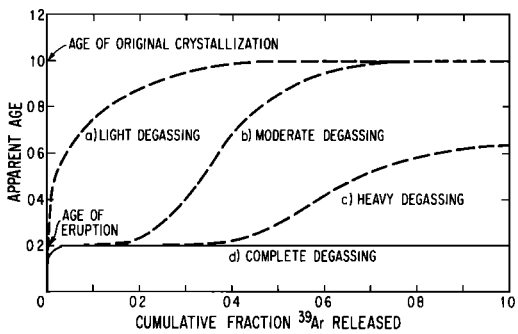

Fig. 2. Schematic ^{40}Ar-^{39}Ar age spectra show increasing depression of apparent age with extent of degassing of ancient xenocrysts in lava during eruption at age 0.2. The original age of crystallization is 1.0. Curves a, b, and c show a progressive decrease in the size of the plateau at age 1.0 and the development of a plateau at age 0.2 as the level of degassing is increased. If degassing is complete (curve d), only an eruption-age plateau is observed. The minor depression in age in the initial releases reflects long-term, low-temperature diffusion loss of $^{40}Ar^*$.

which generally dominates Ar released from the sample at low temperatures. Furthermore, $^{40}Ar_0^*$ remaining in xenocrysts after degassing at 1100°C for many hours in the magma is unlikely to be degassed at lower temperatures in the laboratory. Therefore, it should be possible during ^{40}Ar-^{39}Ar analysis to separate the $^{40}Ar_0^*$ from at least some of the $^{40}Ar^*$ created since cooling of the lava.

1.3 *^{40}Ar-^{39}Ar Analysis of Xenocrysts*

The extent of degassing of Ar from the ancient xenocrysts during heating in the magma depends on characteristics of the xenocrysts, the temperature of the magma, and the time it takes to cool, and determines the shape of the ^{40}Ar-^{39}Ar age spectrum for the xenocryst as shown schematically in Figure 2 and considered in detail in *Gillespie et al.* [1982]. If degassing has been minor, ages for the first fractions of Ar (released at low temperatures) will be less than the age of crystallization and may approach the age of eruption (spectrum a). If degassing has been major, the first fractions of Ar may be extracted free from $^{40}Ar_0^*$, and a plateau giving the age of eruption may be established (spectrum b). If $^{40}Ar_0^*$ from even the most retentive sites has been partially depleted at the time of eruption, the maximum apparent age will be less than the age of crystallization of the xenocrysts (spectrum c). The size of the low-

temperature plateau will increase with the extent of degassing until, for complete degassing, the entire age spectrum reflects the age of eruption (spectrum d).

Because complete degassing of xenocrysts in basaltic magma is not always achieved, we might expect a xenocryst age spectrum characterized by a region of mixed ages separating plateaus giving the ages of crystallization and eruption. If an eruption-age plateau is not found, the minimum apparent age will be an upper limit to the age of eruption, barring irradiation artifacts such as recoil redistribution.

We will demonstrate here the existence of low-temperature plateaus in age spectra of several partially degassed xenoliths and demonstrate their correspondence to the K/Ar age of eruption of the lava that incorporated them. The early Pleistocene basalt chosen for study was found by *Darrow* [1972] to have unusually high levels of K (1.3% by weight). It was thus well suited for K/Ar dating. A relatively old lava flow was chosen to reduce the the sensitivity of the K/Ar age of the basalt to contamination by $^{40}Ar_0$* and to unusual compositions of Ar_t and to increase the extent of the low-temperature plateau in the age spectra of the xenoliths. Xenoliths from this basalt were found by preliminary K/Ar analysis to be ~95% degassed. The results on xenolith sample 1–12 were presented by *Gillespie et al.* [1982] in support of their theoretical study of the conditions under which an eruption-age plateau may be observed.

2. Sample Selection

We chose samples from three sites (Figure 1) where basalt is found on present ridge tops as much as 100 m above the North Fork of Oak Creek. The basalt flows are faulted and are locally capped by eroded remnants of coarse fan deposits. *Darrow* [1972] considered these flows to be among the oldest in the Big Pine volcanic field. The magnetic polarity of the basalt is reversed (D. Van Alstine et al., unpublished data, 1982); thus, its age exceeded 0.73 m.y. [*Mankinen and Dalrymple*, 1979].

At site A, the contact between weathered quartz monzonite of the Cretaceous McGann pluton [*Moore*, 1963] and an overlying nonvesicular basalt is exposed in a road cut. The unusual absence of granitic xenoliths in this basalt suggests that it may have a source separate from the basalts south of Oak Creek at sites B and C. Samples of basalt (NFOC-23a) 10 m above the base of the flow and of quartz monzonite bedrock (NFOC-109) 2 m below the contact were taken at site A. These samples were chosen to explore the possibility of measuring eruption ages by using overridden rock only lightly degassed.

Site B was near the base of the thick (~50 m) sequence of basalt flows that cap the ridge south of Oak Creek. No interbedded fluvial gravels have been found, and the entire sequence may have erupted at about the same time. The sample from site B, NFOC-1, consisted of a large block of basalt containing two 1-cm-diameter granitic xenoliths (NFOC-1a, NFOC-1b). Three pieces of the basalt and duplicates of each xenolith were analyzed.

Site C was at the eroded top of the upper flow. Three samples taken 10 cm below the surface of a 1-m-diameter quartz monzonite xenolith (NFOC-103) (but no samples of basalt) were analyzed.

3. Petrography

The lava from site A is a basanite [*Darrow*, 1972] and contains phenocrysts of olivine and clinopyroxene in a network of smaller laths of plagioclase. Potassium probably resides to some extent in the plagioclase but is found mainly in the small biotite and nepheline crystals reported by Darrow and in ~10-μm glass blebs in the groundmass. Olivine phenocrysts show no iddingsite rims. Granitic xenoliths are rare.

The ridgetop basalt at site B is similar to the basalt at site A, except that in NFOC-1 phenocrysts are larger and more numerous. A few olivine crystals show incipient iddingsite alteration; otherwise, the basalt appears quite fresh. Granitic xenoliths are common, but no isolated xenocrysts were seen in thin sections of NFOC-1 basalt. However, the irregular xenolith interface suggests that some crystals may have been detached from xenolith surfaces.

Most of the granitic xenoliths found in the Oak Creek lavas were probably derived from the McGann quartz monzonite, the pluton exposed in the vicinity of the vents (Figure 1) and overrun by flows at site A. The K-feldspar is microcline, and the dominant mafic mineral is biotite, with subordinate hornblende. At site A the bedrock was weathered before being buried by basalt, and a thin zone of grus was present. This zone was baked by the basalt and is now cemented by iron oxides. Sample NFOC-109 was taken from below this zone, and individual feldspar grains are remarkably fresh appearing, although zones of alteration products can be seen. Plagioclase crystals are sericitized, and mafic minerals are altered, with some replacement by iron oxides. Xenoliths appeared to be distinctly less altered, probably because they were not weathered prior to incorporation in the magma. However, some could be disaggregated by hand, and the xenolith NFOC-103 (site C) showed extensive replacement of biotite and hornblendes by iron oxides, which also pervaded the xenolith along fractures. The 1-cm-diameter xenoliths in NFOC-1 exhibited incipient transformation of K-feldspars from microcline to sanidine, especially at the xenolith-basalt interface. Quartz crystals, as reported by *Moore* [1963] and *Darrow* [1972], were corroded and showed reaction rims of clinopyroxene needles.

4. Analytic Techniques

4.1 *Sample Preparation*

Basalt samples weighing ~0.5 gram were picked from the interior of blocks after coarse crushing. Samples from NFOC-1 were wrapped in metal foil packets to prevent loss during irradiation or loading. It was not necessary to wrap basalt sample 8-12 (from NFOC-23a) in foil. Samples were visually checked for xenocrysts, but none was found.

The granitic bedrock and xenolith samples were gently crushed and sieved. The 104–220-μm fraction was then magnetically cleaned of its mafic minerals to reduce the amount of altered material. Grains of sample 8-3 (from NFOC-103) were etched in 20% HF for 30 s at 25°C to reduce further fine alteration products. Isolated quartz grains were removed from 8-3 by handpicking, so that the sample consisted of etched microcline and plagioclase crystals. All samples were wrapped in foil packets for irradiation. After the first analyses it became obvious that the Ar giving the eruption-age plateaus was released at temperatures between ~500°C and ~900°C, so Sn foil packets were substituted for Al packets in subsequent experiments. This was done to lower the temperature at which air incorporated in the foil was degassed from 660°C to 230°C. Sn and Al foil appeared to degas entirely upon melting.

Samples were irradiated with a fast neutron fluence of $\sim 10^{17}$ n cm^{-2} in the TRIGA reactor facility of the United States Geological Survey at Denver, Colorado. Sample 6-12 (NFOC-1) was irradiated at half this level. Neutron fluence inhomogeneities were monitored by measuring the ^{58}Co γ activity induced in Ni wires placed between samples. The Bern 4M stan-

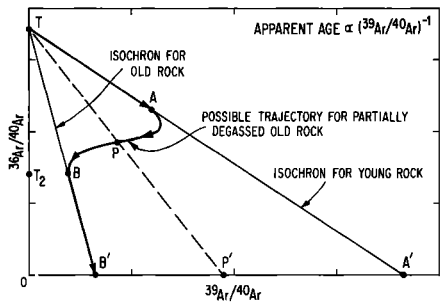

Fig. 3. The three-isotope correlation diagram of $^{36}Ar/^{40}Ar$ versus $^{39}Ar/^{40}Ar$. A linear array in this diagram indicates mixing of a single well-defined trapped Ar component with K-derived Ar of constant composition and hence constant age. Schematic trajectories of the isotopic compositions of Ar released during stepwise heating of degassed xenoliths are drawn to illustrate mixing among different reservoirs of Ar, which may include K-derived Ar accumulated since original crystallization (B'), K-derived Ar accumulated since cooling of the host lava (A'), and trapped Ar (T and T_2). Compositions of K-derived Ar plot on the abscissa; compositions of trapped Ar plot on the ordinate. If only a single composition of trapped Ar is present, trajectories will range within the triangle $TA'B'$.

dard muscovite [*Jäger et al.*, 1963] was used as the neutron irradiation monitor, along with samples of CaF_2 to measure Ca-derived Ar interferences. The age of the muscovite is 17.9 ± 0.6 m.y., the result of ^{40}Ar-^{39}Ar analyses reported by *Dalrymple and Lanphere* [1971] corrected for the recommended ^{40}K abundance and decay constant $\lambda \equiv \lambda_e + \lambda_\beta = 5.543 \times 10^{-10}\ y^{-1}$ [*Steiger and Jäger*, 1977].

4.2 *Argon Analysis*

After neutron irradiation, Ar was extracted from samples in 6–15 1-hour steps at successively higher temperatures from roughly 300°C to 1700°C. Heating was by RF induction in a tungsten crucible vapor-deposited in a helium atmosphere to reduce the Ar blank. Blank Ar was of atmospheric composition. Blank levels of ^{36}Ar ranged from 10^{-10} cm^3 STP at temperatures below 800°C to 10^{-8} cm^3 STP at 1700°C, and temperature intervals between extraction steps were selected to maintain blank levels at <5% of the sample. The Ar extracted from the samples was purified, and then analyzed by using the HENEAK II gas mass spectrometer, with programed magnetic field control. General aspects of the procedure have been published elsewhere [*Radicati et al.*, 1981; *Gillespie*, 1982]. After correction of the measured Ar for interfering isotopes, blank ^{40}Ar and ^{36}Ar were subtracted. Conservative errors of ±50% were assigned to blank levels. Measured blanks were reproducible to ±20%. $^{40}Ar^*/^{39}Ar$ was calculated by subtracting $^{40}Ar_t$ contributions assuming air Ar composition $((^{40}Ar/^{36}Ar)_t = 295.5)$, and apparent ages obtained by using

$$t = \lambda^{-1} \ln (1 + J\ ^{40}Ar^*/^{39}Ar) \quad (1)$$

with $J \equiv (^{40}Ar^*/^{39}Ar)_m^{-1} [\exp(\lambda t_m) - 1]$ determined from the muscovite monitor. Total ages were calculated from (1) by summing the Ar released in all the extractions of the analysis. Plateau ages were calculated by averaging the ages for each step in the plateau weighted by the fraction of ^{39}Ar released. Ages calculated by assuming a value for $(^{36}Ar/^{40}Ar)_t$ are called model ages. To the extent that the composition of the Ar_t is unlike air, the model ages will be inaccurate. To avoid this problem, it would be necessary to know the actual composition of the Ar_t, which may be found by fitting a line to the linear array of compositions plotted in $^{36}Ar/^{40}Ar$ versus $^{39}Ar/^{40}Ar$ diagrams as discussed below. Ages found in this manner will be called isochron ages.

Uncertainties in ages of events must include the 3.5% systematic uncertainty in the age of the muscovite monitor. However, inclusion of this uncertainty is inappropriate if ages referred to the same monitor are to be compared.

4.3 *Data Presentation and Systematics*

We present the isotopic measurements of Ar released by heating during ^{40}Ar-^{39}Ar analysis in two ways: conventional age spectra, in which the apparent age at each step is plotted against the cumulative fractional amount of ^{39}Ar released, and three-isotope variation diagrams, in which the relative amounts and isotopic compositions of trapped and K-derived Ar are made evident. Three-isotope diagrams are especially useful because they show trends in the composition of Ar released at successively higher temperatures. Figure 3 schematically illustrates the use of such diagrams. Ar_t compositions plot on the ordinate and K-derived Ar compositions plot on the abscissa. In general, Ar released from a sample contains both trapped and K-derived Ar and plots along a mixing line connecting the two compositions. Ages are related to $^{39}Ar/^{40}Ar^*$ by (1). The apparent age for Ar from a single extraction step is determined from the abscissa intercept (P') of a line passing through the measured composition (P) and the Ar_t composition (T). If several fractions of Ar released from a sample were mixtures of the same trapped and K-derived components, their linear array of compositions defines an isochron with axis intercepts that specify the composition of the endmembers, which generally cannot be measured directly. The abscissa intercept of the isochron determines an age ('isochron age') for the sample.

Measurement errors and deviation of the real systems from ideal behavior both contribute to uncertainties in the isochrons. If measurement was the main source of error, we used the least squares method of *Williamson* [1968] to estimate the isochron. In this method, individual compositions are weighted according to their measurement precisions. If measurement errors are subordinate, Williamson's method gives unrealistically precise apparent ages because the scatter of compositions about the isochron is not considered. As was recommended by *York* [1969] for such cases, we multiplied the uncertainty of the isochron by $[S/(n-2)]^{1/2}$ where S is the sum of the squares of the residua of data about the isochron and where n is the number of compositions measured. S is distributed as χ^2 with $(n-2)$ degrees of freedom. If S were so large that there was less than 1% chance that the scatter of the compositions about the isochron resulted from measurement uncertainty alone, we took the reduced major axis [*Kermack and Haldane*, 1950] to be the isochron. In this approach the data are not weighted by the measurement uncertainties; the precision of the reduced major axis depends on the correlation coefficient of the isotopic compositions. Because the scatter of compositions about the axis is due to nonexperimental sources, the uncertainty of the age of the isochron must be multiplied by Student's t factor, with $(n-2)$ degrees of freedom [*Brooks et al.*, 1972].

Isochrons shown in Figure 3 connect Ar_t of composition T to K-derived Ar from undisturbed samples of two ages (A' and B'). In the context of this discussion, B' includes $^{40}Ar_0{}^*$ accumulated since original crystallization of the xenocryst, while A' includes only $^{40}Ar^*$ accumulated since the time of eruption. Isochron TA', then, is anticipated for the lava and isochron TB' for the undegassed parent material of the xenocryst. The trajectory of isotopic compositions from the partially degassed xenocryst will range within the triangle $TA'B'$. One possibility is the

TABLE 1. Summary of ^{40}Ar-^{39}Ar Results

Sample	Site	Type	^{40}Ar-^{39}Ar Analysis	Sample Mass, mg	K[a]	Ca[a]	$^{40}Ar^*$ cm^3 STPg^{-1}	^{36}Ar cm^3 STPg^{-1}	$^{39}Ar/^{40}Ar$, $\times 10^3$	$^{36}Ar/^{40}Ar$, $\times 10^5$	Muscovite Monitor, $^{39}Ar/^{40}Ar^*$, $\times 10^4$
NFOC-23a	A	basalt	8-12	378	1.5	6.6	7.5×10^{-8}	3.1×10^{-10}	164	186	241
NFOC-109[b]	A	quartz monzonite	8-10	541	10.1	1.5	$>2.5 \times 10^{-5}$	$>8.0 \times 10^{-9}$	~6	~29	241
NFOC-1	B	basalt	6-12	592	1.3	8.5	4.7×10^{-8}	2.9×10^{-9}	9	321	122
NFOC-1	B	basalt	1-2	744	1.8	9.2	4.4×10^{-8}	1.1×10^{-9}	36	299	243
NFOC-1	B	basalt	1-3	518	1.4	9.8	5.7×10^{-8}	7.5×10^{-10}	75	269	243
NFOC-1a[c]	B	xenolith	1-7	491	4.1	—	$>1.6 \times 10^{-7}$	$>1.9 \times 10^{-9}$	~79	~261	243
NFOC-1a	B	xenolith	1-8	496	3.3	9.2	6.5×10^{-7}	1.5×10^{-8}	9	298	243
NFOC-1b	B	xenolith	1-11	472	>2.8	1.9	$>7.2 \times 10^{-8}$	$>2.7 \times 10^{-9}$	~28	~310	243
NFOC-1b	B	xenolith	1-12	436	3.6	2.9	4.3×10^{-7}	9.1×10^{-9}	10	292	243
NFOC-103	C	xenolith	8-1	88	3.1	1.9	5.7×10^{-7}	1.4×10^{-8}	13	298	241
NFOC-103	C	xenolith	8-2	119	3.4	14.6	5.7×10^{-7}	2.0×10^{-8}	10	309	241
NFOC-103	C	xenolith	8-3	113	2.0	5.1	5.6×10^{-7}	2.0×10^{-8}	6	309	241

[a]Weight percent calculated from ^{39}Ar and ^{37}Ar from sample normalized to isotopes from muscovite and fluorite monitors. Error is ±10%.
[b]Fusion extraction step lost.
[c]400°C extraction step lost.

curving line progressing initially along TA' but deflecting toward B near composition A and progressing finally along TB'. Arrows indicate the trend of compositions as degassing progresses during analysis. Such a trajectory would have an age spectrum similar to spectrum b of Figure 2.

If more than a single composition of Ar_t is present (T and T_2), trends in measured compositions will be more complicated. In the presence of a single K-derived component A', compositions will range within $TA'T_2$, or in the presence of two K-derived components compositions will range within the quadrilateral $TA'B'T_2$. There is no guarantee that a true isochron will be present. Only if the different K-derived or trapped components are derived from sites of sufficiently different Ar retentivity can compositions be expected to lie along binary mixing lines over even part of the trajectory and only if such binary mixing lines are found can ages of events be calculated. The differences in retentivity cannot be known in advance of the analysis. In fact, the efficacy of stepwise heating in isolating binary compositions can only be inferred from the observed trajectory.

5. RESULTS

Results are summarized in Tables 1 and 2. Ages are summarized as total ages, plateau ages, and isochron ages. Uncertainties in the tables and discussion are 2σ; error bars plotted in the figures are 1σ. Complete tabulations of data and details of argon analysis are found in appendixes to this article[1] or in *Gillespie* [1982].

5.1 *Basalt and Subjacent Country Rock From Site A*

We analyzed a sample of quartz monzonite found 2 m below a ~15-m-thick basalt flow. This was done (1) to illustrate the simplicity of trends in isotopic composition of Ar from partially degassed ancient rocks, (2) to illustrate the extreme range of apparent ages calculated from Ar released in different steps, and (3) to help establish guidelines for the selection of xenoliths that have been degassed in the magma sufficiently to permit determination of the eruption age. We also analyzed the overlying basalt, which was free of granitic fragments. This analysis was used to determine the basalt's eruption age and thus the time of degassing of the underlying quartz monzonite.

In Figure 4, trends in the isotopic composition of Ar from the thermally undisturbed basalt are contrasted to those from the subjacent bedrock. Ar from the basalt was extracted in four steps at temperatures from 300°C to 1175°C. The compositions were colinear, indicating a binary mixture of a well-defined Ar_t with K-derived Ar of constant $^{39}Ar/^{40}Ar^*$. Little Ar_t was released from the basalt (3.3×10^{-10} cm^3 STP ^{36}Ar per gram), and even at 300°C the ^{40}Ar was about one-third radiogenic. As the temperature was increased to 900°C, the fraction of $^{40}Ar^*$ increased. This trend was reversed for the 1175°C extraction. The small amount of Ar_t present in the basalt minimized the uncertainty in the age of the basalt due to ill-defined Ar_t composition. The trapped component may have been slightly enriched in ^{40}Ar compared with air Ar since an isochron fit to these data intersected the ordinate at $^{36}Ar/^{40}Ar = 0.00324 \pm 0.00014$. The abscissa intercept of 0.382 ± 0.022 corresponded to an age of 1.13 ± 0.07 m.y., less than the total age of 1.19 ± 0.03 m.y.

The composition of Ar released from the country rock followed a more complicated trajectory. Ar was extracted in eight steps from 300°C to 1700°C. The composition of the first step was near 'AIR.' Subsequent steps plotted near the origin. In the context of Figure 3, the entire trajectory appeared to lie between A and B, with A close to T ('AIR' in Figure 4) and B close to B'. A' and B' are shown in Figure 4 for reference.

The progressive dominance by $^{40}Ar_0^*$ of Ar extracted at increasingly higher temperatures from the poorly degassed quartz monzonite is clearly shown in its age spectrum (Figure 5). The apparent ages monotonically rise with the cumulative fraction of ^{39}Ar released, from ~4 m.y. to 75 m.y. More than 90% of the ^{39}Ar is associated with apparent ages exceeding 50 m.y. The minimum apparent age of ~4 m.y. is an upper limit to the age of the lava; the maximum apparent age of ~75 m.y. is a lower limit to the age of the Cretaceous sample.

5.2 *Degassed Xenoliths and Host Basalt From Site B*

Granitic xenoliths were analyzed to determine if eruption-age plateaus were developed in age spectra of strongly degassed material. Samples for this purpose were taken from the base of

[1] The appendixes are available with the entire article on microfiche. Order from American Geophysical Union, 2000 Florida Avenue, N.W., Washington, D. C. 20009. Document B83-003; $2.50. Payment must accompany order.

TABLE 2. Summary of ^{40}Ar-^{39}Ar Results

^{40}Ar-^{39}Ar Analysis	Model total age, m.y.[a]	Retention,[b] percent	Fraction of ^{39}Ar in Plateau Steps	Number of Steps in Plateau	Model Plateau Age, m.y.[a]	Fraction of ^{39}Ar in Isochron Steps	Number of Steps Fit by Isochron	$\frac{S^c}{n-2}$	Ordinate Intercept of Isochron, $^{36}Ar/^{40}Ar$, $\times 10^5$	Isochron Age, m.y.[a]	Method of Regression[d]
8-12	1.19 ± 0.03	0	1.00	4	1.19 ± 0.04	1.00	4	1.23	324 ± 14	1.13 ± 0.07	W
8-10[e]	61.1 ± 0.9	>67	0	0	—	0	0	—	—	—	—
6-12	1.25 ± 0.08	—	0.80	5	1.23 ± 0.08	0.97	6	1.30	336 ± 1	1.11 ± 0.04	W
1-2	1.41 ± 0.20	—	(0.08)	(1)[f]	(1.31 ± 0.10)	1.00	9	32.92	339 ± 15	1.39 ± 0.15	R
1-3	1.18 ± 0.04	—	0.95	6	1.18 ± 0.02	1.00	8	0.79	342 ± 3	1.20 ± 0.02	W
1-7[e]	1.26 ± 0.16	—	<0.95	6	1.17 ± 0.02	<0.97	7	2.33	333 ± 4	1.15 ± 0.02	W
1-8	6.21 ± 0.30	5	(0.55)	(2)[f]	(1.26 ± 0.03)	0.89	4	14.04	321 ± 17	1.15 ± 0.18	R
1-11[g]	1.32 ± 0.22	>0	~0.76	5	1.23 ± 0.02	1.00	9	12.63	337 ± 11	1.20 ± 0.12	R
1-12	6.29 ± 0.26	6	0.58	8	1.22 ± 0.03	0.58	8	0.87	334 ± 4	1.19 ± 0.02	W
8-1	3.96 ± 0.75	3	(0.37)	(2)[f]	(1.18 ± 0.06)	0.37	3	1.26	338 ± 1	1.17 ± 0.06	W
8-2	3.68 ± 0.18	3	(0.27)	(2)[f]	(1.16 ± 0.02)	0.30	4	6.29	340 ± 13	1.16 ± 0.10	R
8-3	5.93 ± 0.15	3	(0.28)	(2)[f]	(1.29 ± 0.06)	0.46	4	23.44	333 ± 12	1.17 ± 0.16	R

Uncertainties are 2σ.
[a]Uncertainty does not include 3.45% uncertainty in age of Bern 4M muscovite standard.
[b]Assuming xenoliths crystallized 90 m.y. ago, Ar retention ≈ 100 × (total age-eruption age)/90 m.y.
[c]Determined for isochron calculated by Williamson's method.
[d]W = Williamson's method. R = Reduced mean axis.
[e]Fusion extraction step lost.
[f]Too few points to define a true plateau.
[g]400°C extraction step lost.

the basalt flow south of Oak Creek (site B, Figure 1). Two samples from each of two xenoliths found only a few cm apart were analyzed. Three whole-rock basalt samples from the same block (NFOC-1) were analyzed to establish the eruption age.

5.2.1 *Basalt analyses.* $^{36}Ar/^{40}Ar$ versus $^{39}Ar/^{40}Ar$ correlations for the basalt analyses are shown in Figure 6. The top diagram of Figure 6 compares the total Ar compositions of the basalt samples from sites B and A. The compositions are distributed along a 1.18-m.y. reference line drawn through 'AIR.' (1.18 m.y. was chosen because it is the midrange value of isochron ages of the xenoliths in this study (Table 2).) This was due to different concentrations of Ar_t, which varied from 3.3 $\times 10^{-10}$ to 2.9 $\times 10^{-9}$ cm^3 STP ^{36}Ar per gram of basalt (Table 1). Even among the three samples from site B (6-12, 1-2, 1-3), the concentration of ^{36}Ar varied by a factor of 4. Sample 2-15 was powdered before analysis, presumably accounting for its large amount of nonradiogenic Ar (1.4 $\times 10^{-8}$ cm^3 STP ^{36}Ar per gram).

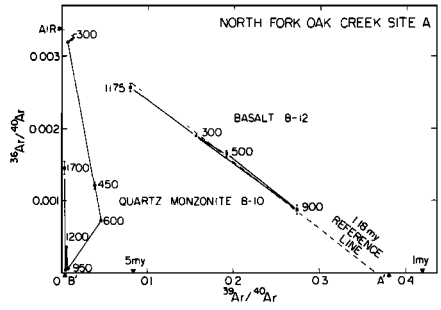

Fig. 4. The correlation of $^{36}Ar/^{40}Ar$ versus $^{39}Ar/^{40}Ar$ for basalt 8-12 shows binary mixing between well-defined K-derived and trapped Ar components. The trajectory for the underlying degassed bedrock 8-10 indicates ternary mixing among two K-derived Ar components (*A'* and *B'*) and a trapped Ar component. A reference line drawn from trapped Ar of atmospheric composition ('AIR') to a K-derived Ar composition corresponding to 1.18 m.y. is included for comparison. Approximate extraction temperatures (°C) are shown for selected steps. Uncertainties are 1σ.

Model ages calculated for the total Ar compositions of two of the basalt samples from site B (1-3 and 6-12) agreed at 1.18 ± 0.04 m.y. and 1.25 ± 0.08 m.y., but the model age of the third sample (1-2) was older at 1.41 ± 0.20 m.y. Because these samples were of the same true age, this discrepancy must be explained either by a variable composition of Ar_t, by local concentrations of $^{40}Ar_0$*, or by loss of ^{39}Ar. Because of the small fraction of ^{40}Ar* in basalts 6-12 and 1-2, the model ages were sensitive to minor errors in the assigned $(^{36}Ar/^{40}Ar)_t$. The model age of basalt 8-12 (1.19 ± 0.03 m.y.) was similar to the model age of basalt 1-3, although each was from a different flow. The fact that ^{40}Ar from 8-12 and 1-3 was rather radiogenic increased our confidence that their model ages gave the actual times of eruption.

The three lower diagrams of Figure 6 show the stepwise degassing results on individual basalts from site B. In general,

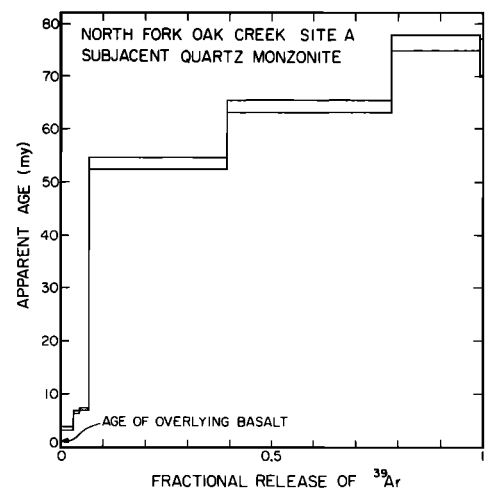

Fig. 5. Model age spectrum of quartz monzonite bedrock 8-10 (calculated assuming 'AIR' trapped Ar composition) shows plateaus at neither the age of original crystallization nor the age of eruption. Model ages of low-temperature steps provide an upper limit of about 4 m.y. to the time of degassing.

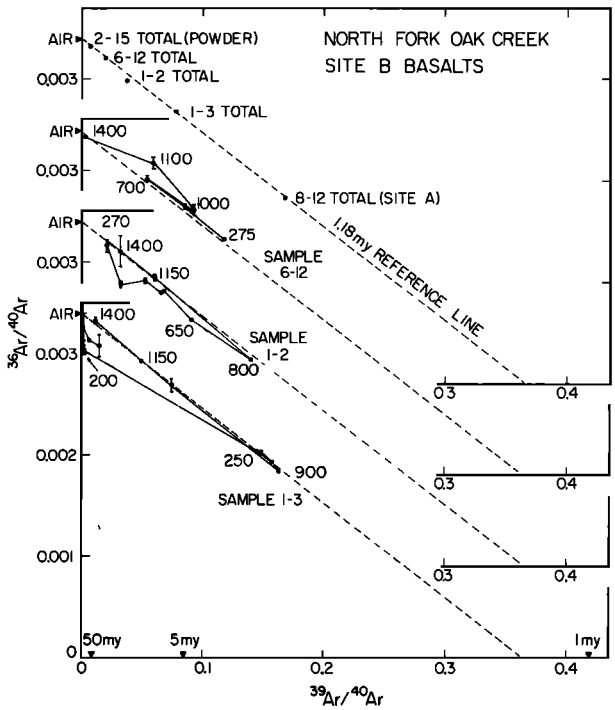

Fig. 6. Ar composition trajectories for basalt samples from NFOC-1 at site B show ternary mixing among two trapped Ar components and a single K-derived Ar component. The top figure shows the composition of all the Ar released from each basalt sample. Failure of the compositions to cluster about a single point reflects variability in the ratio of trapped Ar to K-derived Ar. Differences in trajectories are best attributed to variable amounts of trapped Ar of different compositions. Approximate temperatures (°C) are shown for selected steps.

these trajectories began near 'AIR' and proceeded down the 1.18-m.y. reference line, returning towards 'AIR' at fusion temperatures, as observed for the basalt from site A.

Although total ages and general patterns of isotopic variation were similar for the three basalt samples from site B, each of the trajectories differed in detail. Sample 6-12 was unusual because the most radiogenic Ar was released during the first step (275°C), which accounted for more than 37% of the ^{39}Ar. Ar released in six of the seven steps had colinear compositions close to the reference line. The six colinear steps defined an isochron intersecting the abscissa at an age of 1.11 ± 0.04 m.y. and the ordinate at $(^{36}Ar/^{40}Ar)_t = 0.00336 \pm 0.00001$. Inclusion of the remaining step changed the isochron age to 1.10 ± 0.06 m.y., but raised $S/(n-2)$ and increased from ~75% to >97% the confidence that the scatter in compositions about the fitted line was nonrandom. The trajectory was similar to that expected for a sample containing only two well-defined constituents. There is no evidence for Ar_t of nonatmospheric composition. The single deviant step may reflect recoil redistribution of ^{39}Ar, but because it released only 3% of the ^{39}Ar, it probably does not preclude interpretation of the rest of the trajectory as an isochron.

Ar compositions for sample 1-3 likewise followed a well-behaved trajectory. Ar was released in 12 steps, and 7 of these defined a 1.20 ± 0.02-m.y. isochron intercepting the $^{36}Ar/^{40}Ar$ axis near 'AIR' at 0.00342 ± 0.00003. Ar for the first four steps (<250°C) contained very little ^{39}Ar but ranged from $^{36}Ar/^{40}Ar = 0.00320$ to 0.00304, possibly indicating the presence of a second Ar_t component released without accompanying ^{39}Ar. During the final two steps, Ar was extracted from the molten sample. Compositions from these steps, which together contributed half the Ar_t, plotted near 'AIR' in Figure 6 (the 1650°C post-fusion step is not shown). In the context of Figure 3, compositions ranged within the triangle $TA'T_2$. The component T_2 was present only in small quantities in unretentive sites degassed at low temperatures. Only ~1% of the ^{36}Ar was released in these steps. Compositions of Ar from higher-temperature steps suggested simple mixing between T and A'. Because of the separability of T and T_2, the highly radiogenic content of several of the steps, and the colinearity of compositions at temperatures above 250°C, the isochron age was accepted as the eruption age of the basalt.

In contrast to basalt samples 1-3 and 6-12, compositions of Ar released from basalt 1-2 did not appear to define an isochron. The trajectory of compositions at steps below 800°C was somewhat erratic, with compositions falling well below the isochrons of samples 6-12 and 1-3. However, all fell within the same triangle ($TA'T_2$) defined by sample 1-3. The first six steps appeared to release Ar_t enriched in ^{40}Ar and together accounted for ~40% of the ^{39}Ar. Only at high temperatures (above 1100°C) did Ar compositions plot on the isochrons of samples 6-12 and 1-3. A line fitted to all nine compositions gave an apparent age of 1.39 ± 0.15 m.y., significantly greater than isochron ages for the other two basalts.

5.2.2 *Xenolith analyses.* Three-isotope diagrams for each of the four xenolith samples from site B are shown in Figure 7. Samples 1-7 and 1-8 are from one xenolith, and samples 1-11 and 1-12 are from an adjacent xenolith. As for the basalt samples, compositions appear to range within the triangle $TA'T_2$ (Figure 3). The trajectories for the xenoliths proceeded at low temperatures from an approximately atmospheric

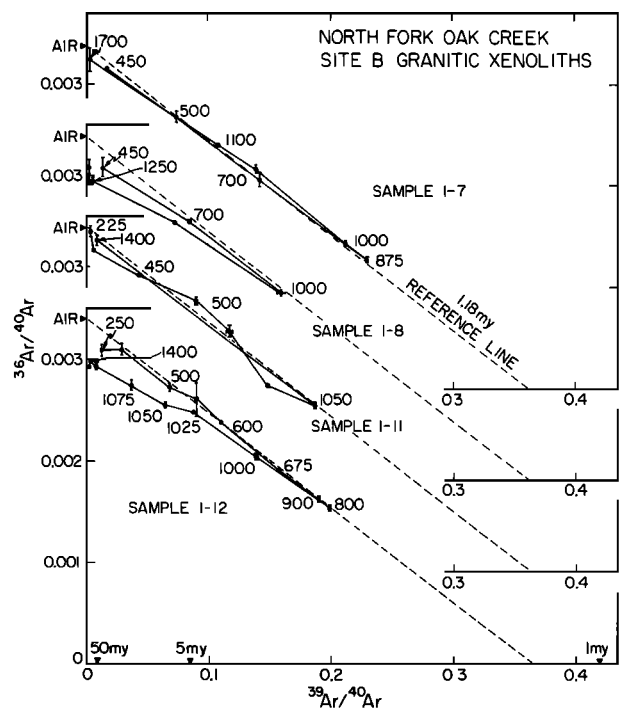

Fig. 7. Ar composition trajectories for granitic xenoliths from site B show ternary mixing. Two Ar components are a trapped Ar near 'AIR' and a K-derived Ar created since degassing in the magma. Compositions of Ar extracted at ~1000°C or less are colinear and define an isochron giving the age of degassing of the xenoliths. Compositions of Ar extracted at higher temperatures probably reflect contributions from $^{40}Ar_0$* not degassed during magmatic heating. Approximate temperatures (°C) are shown for selected steps.

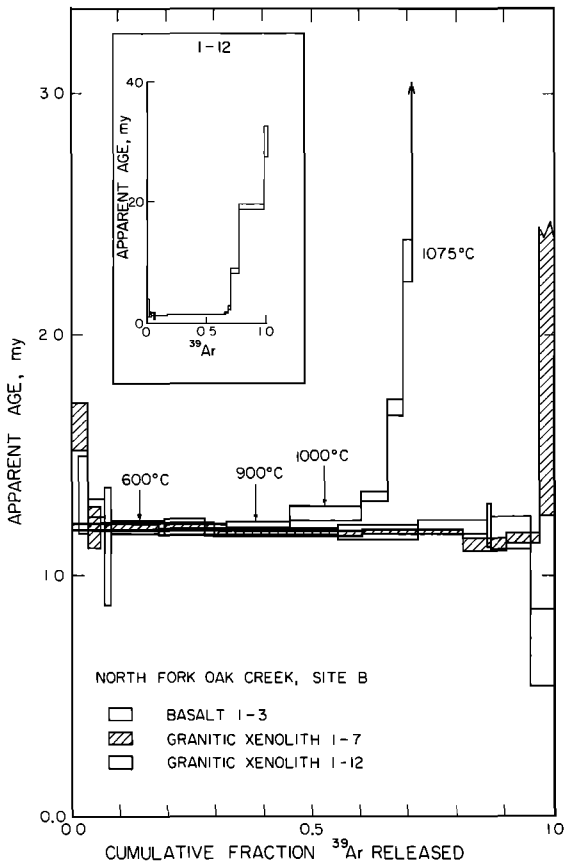

Fig. 8. Age spectra for basalt and two different granitic xenoliths from site B show remarkable agreement for first half of ^{39}Ar released. Plateaus for basalt 1-3 and xenolith 1-7 agree in age over more than 90% of the ^{39}Ar released. Inset shows age spectrum of xenolith 1-12 at a reduced scale to include the high-temperature steps. The rapid increase in age for 1-12 at high temperatures is due to extraction of the $^{40}Ar_0$* remaining after magmatic degassing. Selected approximate extraction temperatures (°C) are shown for sample 1-12. Error bars are $\pm 1\sigma$.

trapped component (T) to the K-derived component (A'), and returned to the ordinate along $A'T_2$ at high temperatures. Ar released from the xenoliths at high temperatures appeared to be enriched by excess ^{40}Ar. Although observed compositions for xenoliths departed from trajectories expected for simple binary systems (TA'), it was not possible from the three-isotope diagrams alone to infer whether the departure at high extraction temperatures was due to the presence of a second Ar_t component (T_2) or to the admixture of $^{40}Ar_0$* from retentive sites. In this latter case, mixing would have occurred within $TA'B'$ rather than $TA'T_2$, but compositions would be restricted to the lines TA and AB, with B plotting close to T.

The four trajectories for site B xenoliths were not identical. Measured compositions for 1-7 were colinear, and Ar_t was released at 1700°C, which was not statistically distinct from air Ar. Ar released from 1-8 at 450°C may have been enriched in ^{40}Ar (or depleted in ^{39}Ar), and Ar released at temperatures above 1250°C was clearly enriched in ^{40}Ar. The trajectory for 1-11 was somewhat erratic but began and ended virtually at 'AIR' and showed no sign of $^{40}Ar_0$*. The initial composition of Ar from 1-12 was excessively radiogenic, while the next seven fractions defined an isochron passing through 'AIR.' As was the case for 1-8, the final several steps were distinctly enriched in ^{40}Ar, defining a mixing line intersecting the ordinate at ~0.0030.

Total ages for the xenoliths were 6.5 m.y. or less, probably corresponding to degassing of 94% or more by the lava. Although the xenolith total ages exceeded the ages for the basalt samples by as much as a factor of 5, it was possible to fit isochrons with small values of $S/(n-2)$ to the Ar compositions by excluding those high-temperature steps that appeared to contain $^{40}Ar_0$*. The abscissa intercepts gave ages clustered around 1.18 m.y. (Table 2). These ages are in excellent agreement both among themselves and with the isochron age of 1.20 ± 0.02 m.y. for basalt 1-3. The different uncertainties in the isochrons reflect the different number of steps free of $^{40}Ar_0$* and also disturbances in the linearity of the Ar compositions. The mean of the isochron ordinate intercepts (weighted by the reciprocal of the variances) indicated $(^{36}Ar/^{40}Ar)_t = 0.00333 \pm 0.00003$, perhaps enriched slightly in ^{40}Ar compared with air Ar.

Figure 8 demonstrates the remarkable agreement among age plateaus from the two different xenoliths and the host basalt. Model ages from xenolith sample 1-7 and from basalt 1-3 agreed within 1σ over more than 90% of the spectrum. (Ar released during fusion of 1-7 was not measured, and abscissa values were calculated assuming that step contained no ^{39}Ar. By comparison with other xenolith samples, it would appear that only ~5% of the ^{39}Ar was released during the fusion step.) Model ages from xenolith 1-12 were within 1σ of model ages of the basalt over the first 60% of the spectrum. Ages calculated from Ar released at temperatures above 1000°C rose rapidly to ~30 m.y. The complete spectrum is shown in the inset, at reduced scale.

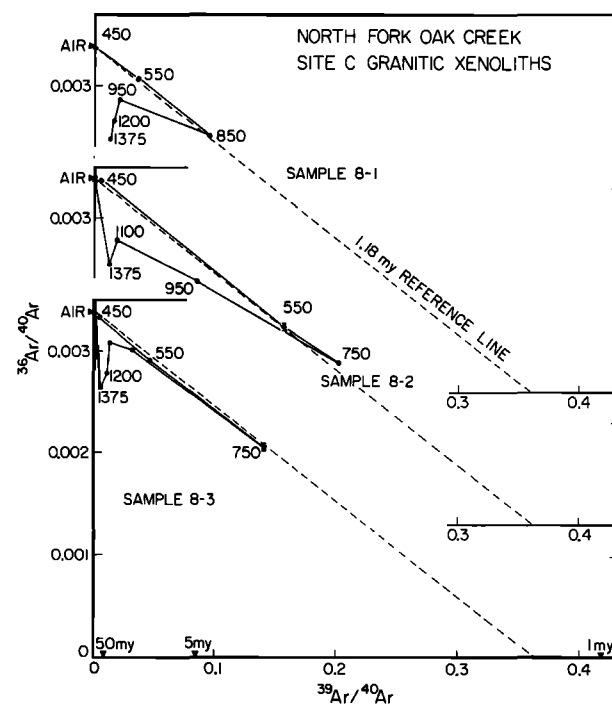

Fig. 9. Ar composition trajectories for xenoliths from site C show the presence of only new ^{40}Ar* at low temperatures but show the clear admixture of residual $^{40}Ar_0$* at temperatures above ~850°C. This admixture is responsible for the trend of the trajectories toward the origin for extractions above 1000°C. Sample 8-3 was etched in HF, and quartz was removed. Approximate temperatures (°C) are shown for selected steps.

5.3 *Degassed Xenoliths from Site C*

A final set of ^{40}Ar-^{39}Ar analyses performed on a xenolith from site C to demonstrate that the appearance of plateaus in the ^{40}Ar-^{39}Ar age spectra of extensively degassed xenoliths was not exceptional. Three fragments were taken from xenolith NFOC-103. From one of these samples (8-3), ~1-mm feldspar grains were handpicked and etched in HF to reduce the amount of altered material analyzed. Other samples were not etched.

Ar trajectories for the three analyses are plotted in Figure 9. Overall, the patterns were distinct from those for all other samples, but closely resembled the predicted trajectory for degassed xenoliths shown in Figure 3. Compositions of Ar released at temperatures below ~1100°C described patterns like those in Figure 7, proceeding from an atmospheric Ar_t toward a K-derived component and returning toward an ordinate intercept somewhat lower than the air value. However, Ar released at the highest temperatures was increasingly radiogenic. In the context of Figure 3, the trajectories seemed to have followed a path from T to A, then returned toward B (located close to T) before ranging from B toward B' and back. Despite the similarity to the model trajectory, compositions of Ar released at high temperatures did not define isochrons. Instead, as for partially degassed country rock (8-10), lines projected from 'AIR' through measured compositions intersected the abscissa increasingly closer to the origin as extraction progressed. The age spectrum of such a pattern resembled curve c of Figure 2. Subsequent fractions included some $^{40}Ar_0$* and corresponded to a region of mixed age.

No trajectory for xenoliths from site C had more than four colinear points. In part, this was because less than 46% of the ^{39}Ar was released before $^{40}Ar_0$* became significant compared with more than 58% from xenoliths from site B. However, isochrons fit to these points gave apparent ages of about 1.17 m.y., close to those from site B.

Plateau ages for the two untreated fragments (Table 2), calculated for Ar released at temperatures of 850°C or less, averaged 1.17 ± 0.04 m.y. This agreed well with ages from the xenoliths and basalt of site B. Although the plateau age of the treated sample (8-3) was 1.29 ± 0.06 m.y., an isochron fit to the first four compositions gave a lower age of 1.17 ± 0.16 m.y., which agreed better with other estimates of the eruption age. Otherwise, the isotopic variation pattern showed no striking differences from the patterns of the untreated samples.

6. DISCUSSION

6.1 *Granitic Xenoliths and Bedrock*

Argon isotopic variation trajectories for the two 1-cm-diameter granitic xenoliths from site B (Figure 8) resembled those for the basalt samples, except that the steps giving the highest apparent ages were taken at the highest temperatures. In contrast, Ar extracted at low temperatures from the basalts was enriched in ^{40}Ar and gave anomalously high ages. Thus, the trajectories were fundamentally different. The excess ^{40}Ar released from the xenoliths at high temperatures above ~1000°C may be explained either by the presence in retentive lattice sites of Ar_t enriched in ^{40}Ar or by the release of $^{40}Ar_0$*. Because the poorly degassed sample of country rock from the same pluton as the xenoliths unmistakably showed the presence of $^{40}Ar_0$*, and because of the clear evidence for $^{40}Ar_0$* in the trajectories of the site C xenolith, we attribute to the release of $^{40}Ar_0$* the departure from binary mixing of the site B xenolith trajectories. Nevertheless, there is an obvious tendency of the trajectories to return to a composition near that of air Ar. The large amounts of ^{36}Ar released during fusion clearly demonstrate the presence of Ar_t in retentive sites in the xenoliths. The amounts of $^{36}Ar_t$ released are 2 orders of magnitude larger than the blank contributions. If the xenoliths indeed contained multiple Ar_t components of different compositions, then their isochrons would have to be interpreted cautiously. More work is needed to resolve this problem, but it does not obviate the dramatic agreement between xenolith degassing ages and basalt eruption ages.

In each of the four xenolith samples from site B more than half of the ^{39}Ar was released in steps with colinear compositions that defined isochrons of the same age (Table 2), even though degassing in the magma was as little as ~94% complete and even though two of the samples (1-8 and 1-12) showed contributions of $^{40}Ar_0$* in steps above 1000°C sufficiently large to raise apparent ages to more than 20 m.y. The isochrons of sample 1-7 and 1-12 (Figure 7) provided the best estimates from xenoliths of the actual age of eruption. Sample 1-7 showed no evidence of $^{40}Ar_0$* at temperatures below fusion, but with a value of $S/(n-2) = 2.33$ may have had scatter in excess of measurement errors. Sample 1-12 had less scatter but a smaller plateau. At 1.15 ± 0.02 m.y. and 1.19 ± 0.02 m. y., these ages were distinct but neither was greatly different from the isochron age of 1.20 ± 0.02 m.y. for basalt sample 1-3.

The age spectrum for xenolith 1-7 demonstrates that if degassing in the magma was nearly complete, the eruption age may be measured from analysis of xenoliths as well as from analysis of the basalt itself. The age spectrum for xenolith 1-12 shows that even if ~6% of the original $^{40}Ar_0$* was retained after degassing by the lava, ^{40}Ar* accumulated since the time of degassing may be completely separated from $^{40}Ar_0$* by stepwise heating and that the eruption age may still be confidently determined.

6.2 *Model Ages and Isochron Ages*

The mean plateau age for all seven xenoliths was 1.22 ± 0.10 m.y. The uncertainty in the mean was almost twice the uncertainty of any individual age. The mean isochron age was 1.17 ± 0.04 m.y., with less than half the uncertainty of the mean plateau age. Only two individual isochron ages had uncertainties smaller than the uncertainty of the mean. Since the xenoliths were degassed in the magma at about the same time, the reduced scatter in isochron ages is perhaps best explained by different compositions of Ar_t.

Ordinate intercepts of the seven xenolith isochrons indicate that the mean $(^{36}Ar/^{40}Ar)_t$ was 0.00335 ± 0.00018. This value is not statistically different from atmospheric Ar (0.00338), but at the 95% confidence level four of the isochrons did have nonatmospheric ordinate intercepts. If Ar_t had a nonatmospheric composition, then model ages are inaccurate and isochron ages must be used to determine the actual age of events.

The best estimate of the age of degassing of the xenoliths is probably the mean of the individual isochron ages weighted by their variances. The mean ages are 1.17 ± 0.01 m.y. and 1.17 ± 0.05 m.y. for the xenoliths from sites B and C, respectively, and are indistinguishable both from each other and from the weighted mean age of 1.18 ± 0.02 m.y. found for basalt samples 1-3 and 6-12. Thus, these ages may be pooled. Including Student's t factor and the systematic uncertainty for the Bern 4M monitor, the weighted mean age of degassing for all nine samples from sites B and C is 1.18 ± 0.05 m.y.

6.3 *Recoil Redistribution of ^{39}Ar*

Recoil of ^{39}Ar during neutron irradiation does not appear to have upset the correlation of $^{40}At^*$ and ^{39}Ar in any of the samples. *Huneke and Smith* [1976] observed significant recoil of ^{39}Ar from μm-sized grains, and because most K in basalts probably resides in crystals and shreds of glass less than 50 μm in diameter, at least some effects were anticipated. Because of the larger potassic grains, recoil distribution should be minor in the granitic xenoliths. Although the possible distortions of the composition trajectories are numerous, one commonly observed effect of recoil is a deficiency of ^{39}Ar in Ar extracted at low temperatures and an excess at high temperatures. Ar released from basalt 8-12 at both low and high temperatures was less radiogenic than Ar released at intermediate temperatures. Thus, the effect of recoil redistribution of ^{39}Ar could have been a reduction in the colinearity of compositions rather than a systematic change in the slope of the trajectory. Too few steps were taken in the analysis of basalt 8-12 to rule out recoil redistribution, but the observed colinearity of compositions suggests that any effects were minor. The apparently high model age of the 1175°C step could imply a deficiency of ^{39}Ar in Ar extracted at high temperatures and is therefore not readily explained by recoil. A more satisfactory explanation is the ^{40}Ar-rich composition of Ar_t indicated by the isochron or the presence of $^{40}Ar_0^*$ from undetected xenocrysts (Figure 4, Table 2).

6.4 *Trapped Argon*

Interpreting Ar composition variations in terms of isochrons depends on the assumption that the measured Ar is a mixture of only one trapped and one K-derived end member. We found that appreciable quantities of ^{36}Ar were released at all temperatures during analyses of both basalts and granitic xenoliths and interpreted this to mean that Ar was trapped within mineral lattices during crystallization [*Frechen and Lippolt*, 1965; *Musset and Dalrymple*, 1968; *Lanphere and Dalrymple*, 1971] as well as adsorbed onto grain surfaces. While the latter was presumably atmospheric in composition, Ar_t in the lattice need not have been. Thus, it is possible that more than two end-member compositions were present. However, our results and the theoretical considerations of *Gillespie et al.* [1982] suggest that even in the presence of multiple end members reliable ages may be deduced, as long as within some temperature range only one trapped and one K-derived Ar reservoir are tapped.

In basalts with negligible $^{40}Ar_0^*$, the Ar isotopic compositions during stepwise release might begin at one Ar_t end member, proceed toward the single K-derived end member, and return to to a different Ar_t end member. The release of Ar_t after reservoirs of K-derived Ar are largely depleted appears to be common for many different rocks and minerals [cf. *Jessberger et al.*, 1974; *Brereton*, 1972]. Inference of an eruption age requires the Ar_t end members to be thermally separable, so that the trajectory of Ar compositions contains linear segments. Basalt 1-2 released Ar whose compositions appeared to result from ternary mixing; however, the requisite linear arrays of compositions were not observed, and a reliable age could not be determined.

In xenoliths with significant amounts of $^{40}Ar_0^*$ and multiple Ar_t reservoirs, Ar compositions would range within a quadrilateral in the three-isotope diagram. It is unlikely that the isotopic variation pattern could be clearly interpreted over its whole course. Identification of an eruption-age isochron would depend upon thermal release characteristics of $^{40}Ar_0^*$ as well as separation of the trapped components.

Multiple reservoirs of Ar_t (of whatever composition) were indicated by the ^{36}Ar release patterns for the xenoliths. This is clearly displayed in Figure 10, which contrasts the release patterns of ^{36}Ar to those of ^{37}Ar, ^{39}Ar, and $^{40}Ar^*$ for xenolith

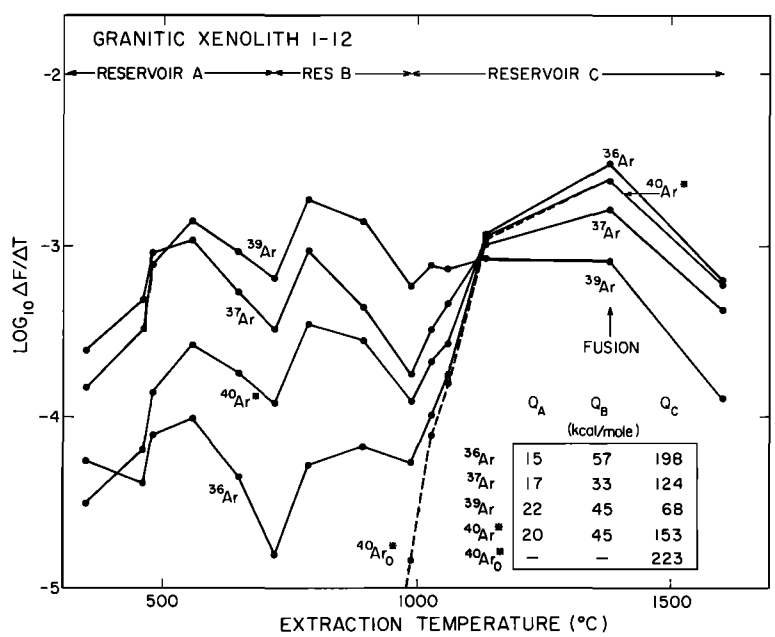

Fig. 10. Ar release patterns for xenolith sample 1-12. The fraction of Ar (ΔF) released at each extraction temperature was normalized by the change in temperature (ΔT) between extraction steps. (Temperatures are effective temperatures compensated for extraction time irregularities and for recorded fluctuations in the induction furnace current.) The dashed curve shows $\Delta F/\Delta T$ for $^{40}Ar_0^*$ retained during degassing in the lava. Ar was released from at least three distinct reservoirs. The prominent rise in $\Delta F/\Delta T$ for $^{40}Ar^*$ and ^{36}Ar compared with ^{39}Ar and ^{37}Ar in reservoir C is attributable to Ar not lost from retentive sites during heating in the host lava. Apparent activation energies Q shown in the box below the curves were calculated from Ar released in each peak.

sample 1-12. Amounts of each Ar isotope released during each extraction step have been normalized by the total amount of that isotope in the sample and by the temperature difference between steps. This was done to reduce the effect of irregularities in the heating schedule on the release patterns. The temperature range of major Ar release from a reservoir during analysis is controlled by an activation energy Q and diffusion parameter D_0/a^2, where a is characteristic radius for Ar diffusion. A curve describing gas released from uniform grains rises with extraction temperature until the reservoir begins to deplete significantly, whereupon the curve reverses slope. Each reservoir in a system is characterized by its own peak, although separation of the peaks need not be sufficient to permit unambiguous identification of each.

In sample 1-12 (Figure 10) there appear to be three separate reservoirs, characterized by different Q and D_0/a^2, which release Ar over different temperature ranges. The amounts of ^{37}Ar and ^{39}Ar in each reservoir are about the same, while $^{40}Ar^*$ and ^{36}Ar are dominated by gas released from the most retentive reservoir. Because ^{36}Ar exceeded blank levels by an order of magnitude or more in most extraction steps, the ^{36}Ar release pattern clearly reflects a characteristic of the xenolith. We have attributed the increase in $^{40}Ar^*$ to $^{40}Ar_0^*$ remaining in the xenolith upon cooling of the host lava. ^{36}Ar trapped during original crystallization was probably also partially retained.

^{37}Ar and ^{39}Ar are created during neutron irradiation and are not subject to degassing by the magma. Apparent activation energies calculated for these two isotopes are largest for the high-temperature reservoir, but in no case do the activation energies exceed those cited for feldspars [e.g., *Gerling and Morozova*, 1962]. In contrast, the activation energy calculated for the high-temperature reservoir 'C' of $^{40}Ar_0^*$ is about 220 kcal/mole. ($^{40}Ar^*$ created in the 1.2 m.y. since eruption is subtracted from the measured amounts so that only $^{40}Ar_0^*$ is considered.) The activation energy for $^{40}Ar_0^*$ is over three times that of ^{39}Ar from the same reservoir. ^{36}Ar likewise shows a large activation energy of roughly 200 kcal/mole for the high-temperature reservoir 'C'. To illustrate one possible explanation for these high activation energies, we have generated Arrhenius plots for diffusion from identical spheres subjected to different amounts of degassing but treated as if none had occurred, as was done to calculate the activation energies from the experimental data. The results of the model calculation are shown in Figure 11. It is evident that the effect of only 20% degassing is practically to double the apparent activation energy calculated from the Arrhenius plot. This apparent activation energy is insensitive to changes in the amount of degassing if the reservoir is largely depleted. Thus, the high apparent activation energies for ^{36}Ar and ^{40}Ar calculated for sample 1-12 indicate that both ^{36}Ar and ^{40}Ar released at high temperatures (reservoir 'C') were residua from degassing in the lava. Consistent with this, we note that more ^{36}Ar was released at high extraction temperatures from xenolith 1-12, which was 6% retentive of $^{40}Ar^*$, than from xenolith 1-11, which showed no $^{40}Ar_0^*$ at all. The existence of xenolith isochrons with air Ar_t intercepts defined by Ar released from NFOC-1 at temperatures below ~1000°C (Figure 7) and from NFOC-103 below ~850°C (Figure 9) demonstrate that if strongly nonatmospheric Ar_t components were present in the xenoliths, they occupied only retentive sites, together with $^{40}Ar_0^*$, and their influence on the inferred age of eruption was negligible. Ar_t released from xenoliths at low temperatures was probably air Ar adhered to surfaces or incorporated during incipient weathering or alteration; Ar_t released at high temperatures was presumably trapped in the xenolith at the time of original crystallization. The presence of $^{40}Ar_0^*$ in Ar released at high temperatures masks the composition of Ar_t from retentive sites, but we must in general consider the possibility that Ar_t released at different temperatures has different compositions. However, the chief opportunities for Ar_t complexity in the Ar release patterns occur when the release of $^{40}Ar_0^*$ already precludes interpretation of step ages as dates, and generally only the composition of the Ar_t released at low temperatures will have an effect on the apparent eruption age. In all cases, original Ar_t should have diffused out of the grains from those sites which also lost $^{40}Ar_0^*$. That portion of the Ar composition trajectory corresponding to the eruption-age plateau in the age spectrum should generally lie on a mixing line connecting $^{40}Ar^*$ to Ar_t introduced into the xenolith since cooling of the lava.

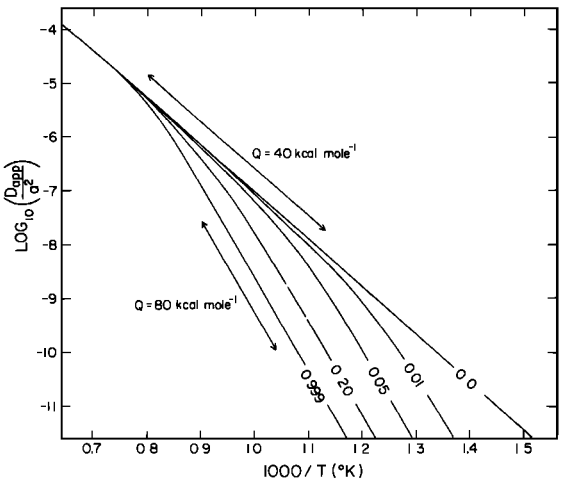

Fig. 11. Arrhenius diagrams for spheres degassed of different fractions F of ^{40}Ar immediately before analysis. For the examples shown, ^{40}Ar extracted during analysis was calculated assuming $D = 50 \exp[-4 \times 10^4/(RT)]$, extraction steps lasting one hour, and a temperature increment of 0.1 K between steps in all cases. The apparent diffusivity, D_{app}, was calculated at different temperatures as though $F = 0$. Degassing before analysis resulted in a reduction of D_{app} at low temperatures and convex curves instead of straight lines. The apparent value of Q, found from the slope of the straight line relating $\log (D/a^2)$ to T^{-1}, was increased from its actual value of 40 kcal/mole to a maximum of ~80 kcal/mole. The high values of Q calculated for ^{40}Ar and ^{36}Ar extracted from xenoliths at high temperatures (Figure 10) may thus be explained by partial loss of Ar from the retentive phases during degassing in the lava.

7. CONCLUSIONS

We have measured the age of eruption of a Pleistocene basalt by ^{40}Ar-^{39}Ar stepwise analysis of the host basalt and of granitic xenoliths originally crystallized more than 75 m.y. ago. The existence of low-temperature plateaus in age spectra of the xenoliths and the good agreement of these plateau ages with model and isochron ages of the host basalt establishes ^{40}Ar-^{39}Ar analysis of xenoliths as a useful method of dating the eruption of the host lava. The identification of granitic xenoliths as appropriate material for ^{40}Ar-^{39}Ar dating is significant because it permits measurement of eruption ages for young lavas that would otherwise be difficult to date.

From the excellent agreement between isochron ages derived for these different systems, we conclude that the weighted mean apparent age of 1.18 ± 0.05 (2σ) m.y. is the eruption date of the basalt capping the ridge south of the North Fork of Oak Creek.

Ages obtained from xenoliths from the base and at the eroded top of the basalt flows south of the North Fork of Oak Creek were indistinguishable. Apparently, the ~50-m-thick sequence of flows was erupted within a short period of less than ~0.1 m.y. It was necessary to use isochron ages because of the presence of trapped Ar enriched in ^{40}Ar compared with air Ar.

Multiple reservoirs of trapped Ar were shown to exist in both the basalt and the xenoliths. In the basalt, at least two trapped components of different composition appeared to be present. The resulting disagreement of model total ages of adjacent samples emphasized the unreliability of conventional K/Ar analysis for dating complicated systems. The presence of multiple trapped components of different compositions necessitates dating young samples by the multiple stage, thermal release method of ^{40}Ar-^{39}Ar analysis.

Only a small fraction of the Ar in the xenoliths was retained after heating in the lava, and the low-temperature plateaus in the age spectra encompassed a large fraction of the ^{39}Ar released. According to *Gillespie et al.* [1982], if the xenoliths had degassed in the magma as identical spheres, the amount of original $^{40}Ar^*$ that was retained would have been sufficient to preclude the development of low-temperature plateaus; the extensive eruption-age plateaus actually observed are characteristic of diffusion models with two or more sites of different dimensions or activation energies. The behavior of such models coupled with the present results suggests that the technique of dating lavas by analyzing xenoliths can be successfully applied to yet younger lavas.

Acknowledgments. Filippo Radicati di Brozolo assisted during early ^{40}Ar-^{39}Ar analyses and gave unstintingly of his time and advice. Theodore Wen measured K concentrations for several preliminary samples. We thank G. Brent Dalrymple and Derek York for their thoughtful criticisms of the article. This research was supported by NSF grants EAR 78-01787 and EAR 79-19997. Contribution 3506 (364) of the Division of Geological and Planetary Sciences, California Institute of Technology.

REFERENCES

Brereton, N. R., A reappraisal of the $^{40}Ar/^{39}Ar$ stepwise degassing technique, *Geophys. J. R. Astron. Soc., 27*, 449–478, 1972.

Brooks, C., S. R. Hart, and I. Wendt, Realistic use of two-error regression applied to rubidium-strontium data, *Rev. Geophys. Space Phys., 10*, 551–577, 1972.

Dalrymple, G. B., Potassium-argon dates of three Pleistocene interglacial basalt flows from the Sierra Nevada, California, *Geol. Soc. Am. Bull., 75*, 753–758, 1964*a*.

Dalrymple, G. B., Argon retention in a granitic xenolith from a Pleistocene basalt, Sierra Nevada, California, *Nature, 201*, 282, 1964*b*.

Dalrymple, G. B., and M. A. Lanphere, $^{40}Ar/^{39}Ar$ technique of K-Ar dating: A comparison with the conventional technique, *Earth Planet. Sci. Lett., 12*, 300–308, 1971.

Dalrymple, G. B., R. M. Burke, and P. W. Birkeland, Concerning K-Ar dating of a basalt flow from the Tahoe-Tioga interglaciation, Sawmill Canyon, southeastern Sierra Nevada, California, *Quat. Res., 17*, 120–122, 1982.

Darrow, A. C., Origin of the basalts of the Big Pine volcanic field, California, Master's Thesis, Univ. of Calif. at Santa Barbara, 1972.

Frechen, J., and H. J. Lippolt, Kalium-Argon Daten zum Alter des Laacher Vulkanismus der Rheinterrassen und der Eiszeiten, *Eiszeitalter Ggw., 16*, 5–30, 1965.

Gerling, E. K., and I. M. Morozova, Determination of the activation energy for the release of argon and helium from minerals, *Geochemistry, 12*, 1255–1268, 1962.

Gillespie, A. R., Quaternary glaciation and tectonism in the southeastern Sierra Nevada, Inyo County, California, Ph.D. Thesis, Calif. Inst. of Tech., Pasadena, Calif., 1982.

Gillespie, A. R., J. C. Huneke and G. J. Wasserburg, An assessment of ^{40}Ar-^{39}Ar dating of incompletely degassed xenoliths, *J. Geophys. Res., 87*, 9247–9257, 1982.

Huneke, J. C., and S. P. Smith, The realities of recoil: ^{39}Ar recoil out of small grains and anomalous age patterns in ^{39}Ar-^{40}Ar dating, *Proc. Lunar Sci. Conf., 7*, 1987–2008, 1976.

Jäger, E., E. E. Niggli, and H. Baethge, Two standard minerals, biotite and muscovite, for Rb-Sr and K-Ar age determinations, sample Bern 4B and Bern 4M from a gneiss from Brione, Valle Verzasca (Switzerland), *Schweiz. Mineral. Petrog. Mitt., 43*, 465–470, 1963.

Jessberger, E. K., J. C. Huneke, F. A. Podosek, and G. J. Wasserburg, High resolution argon analysis of neutron-irradiated Apollo 16 rocks and separated minerals, *Geochim. Cosmochim. Acta, Suppl. 5, 2*, 1419–1449, 1974.

Kermack, K. A., and J. B. S. Haldane, Organic correlation and allometry, *Biometrika, 37*, 30–41, 1950.

Knopf, A., A geologic reconnaissance of the Inyo Range and the eastern slope of the southeastern Sierra Nevada, California, with a section on the stratigraphy of the Inyo Range by Edwin Kirk, *U.S. Geol. Survey Prof. Paper 110*, 130 pp., 1918.

Lanphere, M. A., and G. B. Dalrymple, A test of the $^{40}Ar/^{39}Ar$ age spectrum technique on some terrestrial materials, *Earth Planet. Sci. Lett., 12*, 359–372, 1971.

Mankinen, E. A., and G. B. Dalrymple, Revised geomagnetic polarity time scale for the interval 0–5 m.y. B. P., *J. Geophys. Res., 84*, 615–626, 1979.

Merrihue, C. M., and G. Turner, Potassium-argon dating by activation with fast neutrons, *J. Geophys. Res., 71*, 2852–2857, 1966.

Moore, J. G., Geology of the Mount Pinchot quadrangle, southern Sierra Nevada, California, *U.S. Geol. Survey Bull. 1130*, 152 pp., 1963.

Musset, A. E., and G. B. Dalrymple, An investigation of the source of air Ar contamination in K-Ar dating, *Earth Planet. Sci. Lett., 4*, 422–426, 1968.

Radicati de Brozolo, F., J. C. Huneke, D. A. Papanastassiou, and G. J. Wasserburg, ^{40}Ar-^{39}Ar and Rb-Sr age determinations on Quaternary volcanic rocks, *Earth Planet. Sci. Lett., 53*, 589–597, 1981.

Steiger, R. H., and E. Jäger, Subcommision on Geochronology: Convention on the use of decay constants in geo- and cosmochronology, *Earth Planet. Sci. Lett., 36*, 359–362, 1977.

Turner, G., Argon 40/argon 39 dating of lunar rock samples, *Geochim. Cosmochim. Acta, Suppl. I, 2*, 1665–1684, 1970.

Turner, G., ^{40}Ar-^{39}Ar ages from the lunar maria, *Earth Planet. Sci. Lett., 11*, 169–191, 1971.

Williamson, J. H., Least-squares fitting of a straight line, *Can. J. Phys., 46*, 1845–1847, 1968.

York, D., Least-squares fitting of a straight line with correlated errors, *Earth Planet. Sci. Lett., 5*, 320–324, 1969.

(Received August 13, 1982;
revised March 1, 1983;
accepted March 1, 1983.)